Distribution of present-day vertical deformation across the Southern Alps, New Zealand, from 10 years of GPS data

J. Beavan,[1] P. Denys,[2] M. Denham,[2] B. Hager,[3] T. Herring,[3] and P. Molnar[4]

Received 31 May 2010; revised 30 June 2010; accepted 7 July 2010; published 21 August 2010.

[1] We use ten years of GPS data from nine continuous and six semi-continuous GPS stations in a transect across the Southern Alps to measure rates of relative vertical movement with typical 1σ uncertainties of 0.3–0.5 mm/yr. The estimated vertical rates define a fairly smooth profile across the range, with the highest rates of ~5 mm/yr found near the crest of the mountains and ~20–30 km southeast of the Alpine Fault. The distribution of vertical rates supports models based on horizontal velocities from GPS surveys in which interseismic coupling on the Alpine Fault decreases from 100% near the surface to zero by 13–18 km depth. **Citation:** Beavan, J., P. Denys, M. Denham, B. Hager, T. Herring, and P. Molnar (2010), Distribution of present-day vertical deformation across the Southern Alps, New Zealand, from 10 years of GPS data, *Geophys. Res. Lett.*, *37*, L16305, doi:10.1029/2010GL044165.

1. Introduction

[2] The recognition of plate tectonics brought an appreciation for large horizontal movements on the Earth's surface, and the development of space geodesy brought the means to quantify them. Rates of vertical motion are harder to estimate, in part because they are lower but also because they are more difficult to measure. Moreover, vertical movements of rock and survey control points respond to a number of processes, including erosion of adjacent rock and its isostatic compensation, which complicates the interpretation of vertical movement. It follows that accurate measurement of vertical ground motion should help resolve the relative importance of geodynamic and other processes, including isostatic response to erosion.

2. Southern Alps Tectonic Setting

[3] Since ~20 Ma the central South Island of New Zealand (Figure 1) has deformed in response to oblique continental convergence [*Cande and Stock*, 2004] with one result being the formation of the Southern Alps. The present-day and 3-Myr-average relative plate velocities are each ~39 mm/yr, with a shortening component normal to the Alpine Fault of 6–9 mm/yr [*DeMets et al.*, 2010; *Beavan et al.*, 2002].

[4] High levels of shallow and intermediate depth seismicity define the subduction zones north and south of the Southern Alps, but only scattered minor seismicity occurs within the region of oblique convergence in the central South Island. Most is confined to the upper 10–12 km [*Leitner et al.*, 2001], but a few deeper events are consistent with some brittle deformation in the uppermost mantle [*Reyners*, 1987; *Kohler and Eberhart-Phillips*, 2003].

[5] Paleoseismic and geological studies have shown the central portion of the Alpine Fault to rupture with displacements of 4–8 m in major earthquakes every few hundred years, with an average slip rate of 25–30 mm/yr. No rupture has been recorded historically, but the most recent event is believed from tree-ring and other studies to have occurred in 1717 [e.g., *Sutherland et al.*, 2007]. Approximately 10 mm/yr of the right-lateral component of plate motion occurs off the Alpine Fault, and is thought to occur mostly on faults distributed through the mountainous terrain to the southeast.

[6] *Wellman* [1979] inferred vertical rates of up to 10 mm/yr from measurements of Quaternary faulting along the Alpine Fault and corrections for sea level changes, and from extrapolations of apparent tilting of lake shorelines. Estimates based on geochronological data [e.g., *Batt and Braun*, 1999] suggest rock exhumation rates up to ~10 mm/yr.

[7] Several seismic, magnetotelluric and geodetic experiments over the past 15 years have probed the structure and deformation of the Southern Alps [see *Okaya et al.*, 2007]. These studies quantify the pronounced asymmetry to the deformation, with the most rapid shortening, vertical movement, and erosion occurring in crust east of the Alpine Fault, but west of the axis of the Southern Alps. The initial asymmetry was perhaps due to an inherited weak zone at the position of the Alpine Fault [*Sutherland et al.*, 2000], but it has been emphasized by feedback between climate and tectonics due to the high rainfall and erosion on the western side of the mountains [*Koons*, 1989].

[8] Both gravity and active seismic data define a pronounced root to the Southern Alps that extends to ~40 km depth, compared to 20–25 km crustal depths near the coasts. The root lies some 10–20 km south-east of the topographic crest of the range, and its depth is greater than needed to balance the Southern Alps isostatically, suggesting a mass excess in the upper mantle [*Stern et al.*, 2000].

[9] Magnetotelluric data suggest a high-conductivity region at depths below 5 km on the southeastward dipping Alpine Fault, and an extensive region of high conductivity at depths of 20–30 km above the crustal root. This region is interpreted as a locus of fluid production from prograde metamorphism of cooler crustal material as it is advected downward in the root [*Wannamaker et al.*, 2002]. A

[1]GNS Science, Lower Hutt, New Zealand.
[2]School of Surveying, Otago University, Dunedin, New Zealand.
[3]Earth, Atmospheric, and Planetary Sciences, Massachusetts Institute of Technology, Cambridge, Massachusetts, USA.
[4]Department of Geological Sciences and Cooperative Institute for Research in Environmental Science, University of Colorado at Boulder, Boulder, Colorado, USA.

0094-8276/10/2010GL044165

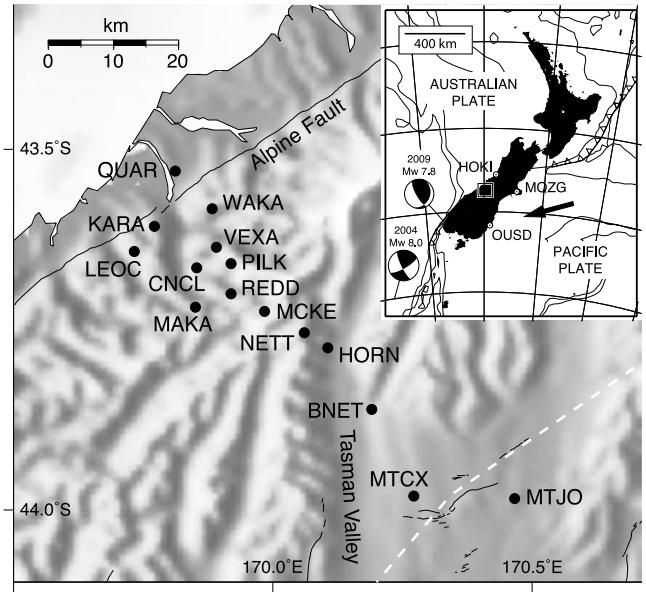

Figure 1. GPS sites superimposed on shaded relief map of central Southern Alps, with main map location indicated by white rectangle on inset. Arrow on inset shows 39 mm/yr Pacific-Australia relative plate motion vector. Black lines are faults from the 1997 version of the GNS Active Faults Database. Block boundaries used by *Wallace et al.* [2007] are the Alpine Fault and the dashed white line through the southeastern foothills.

northwest dipping high conductivity region extending towards the surface on the eastern side of the mountains supports the inference of a two-sided mountain belt [e.g., *Beaumont et al.*, 1996].

3. Experiment Design

[10] Four years of survey-mode GPS [*Beavan et al.*, 1999], even with a 2002 survey extending the data span to 8 years, were insufficient to estimate reliable vertical rates across the Southern Alps. We therefore installed a GPS network to measure these rates [*Beavan et al.*, 2003]. The permanent geodetic monument at most sites (Figure 1) is a short (~0.5 m) reinforced concrete pillar well anchored into bedrock, with a small stainless steel plate and thread set in its top for repeatable mounting of the GPS antenna. The continuous sites record data as 30-s samples, while the semi-continuous sites record 60-s samples to limited internal memory. The latter are downloaded manually every 3 months and then usually moved to a different site. Due to constraints such as snow cover at higher elevations semi-continuous sites are sometimes occupied for consecutive 3-month periods. As far as possible, the same antenna is used at the same site (Table S1 in Text S1 of the auxiliary material).[1] With time we have added continuous sites and converted some semi-continuous sites to continuous recording. We have measured vertical rates at 15 sites in the Southern Alps using 12 GPS receivers, and also at two continuous sites (OUSD, MQZG) on the east coast and one on the west (HOKI) to provide constraints on vertical rates far from the main transect.

[1]Auxiliary materials are available in the HTML. doi:10.1029/2010GL044165.

4. GPS Processing and Time Series Analysis

[11] We analyze the GPS data with Bernese v5.0 software [*Dach et al.*, 2007] to generate daily solutions using fixed orbits in the ITRF2000/IGb00 reference frame with several regional IGS stations constrained to their IGb00 positions and velocities. The resulting vertical component time series contain substantial common-mode noise that we reduce by regional filtering [*Wdowinski et al.*, 1997], implemented in combination with outlier rejection as by *Beavan* [2005]. We analyze the filtered series (Figure 2) by a maximum likelihood method [*Williams et al.*, 2004; *Williams*, 2008] that simultaneously estimates linear displacement rates (Table 1), offsets at specified times (Table S1), seasonal cycles (Table S2), and power-law and white noise parameters (Tables 1 and S3), together with realistic uncertainty estimates. For these regionally filtered time series the noise structure is usually whiter than the flicker noise characteristic of global GPS time series [e.g., *Williams et al.*, 2004; *Beavan*, 2005], with the estimated power-law exponent ranging from −0.3 to −1.3. 1σ uncertainties are 0.9 mm/yr or lower at all stations

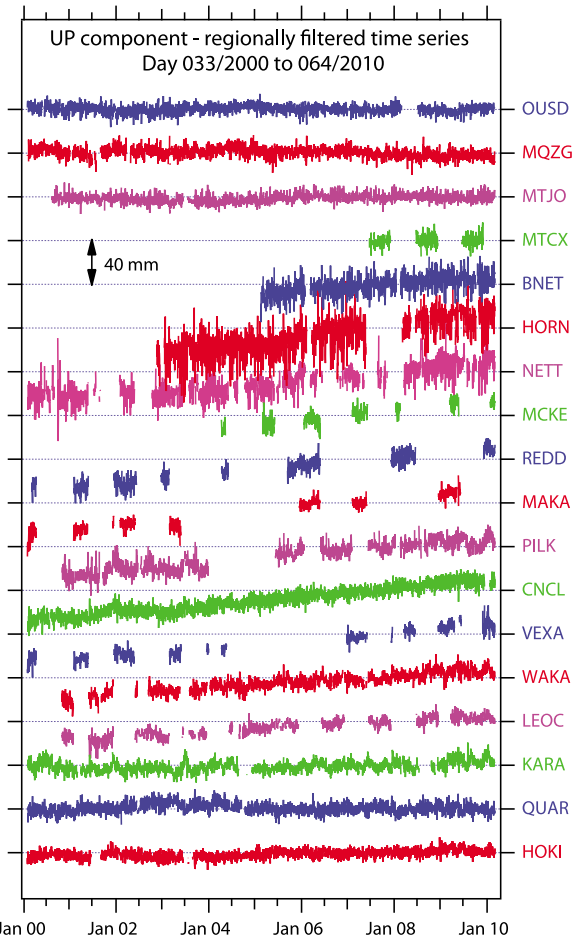

Figure 2. Time series of vertical position, with a small constant slope added to all series to make the OUSD rate equal to zero.

Table 1. Vertical Rate Estimates

Site[a]	Distance From AF (km)	Power-Law Index	Rate[b] (mm/yr)
HOKI	−25.8	−0.7	0.7 ± 0.2
QUAR	−2.9	−0.8	0.1 ± 0.2
KARA	2.4	−1.1	0.9 ± 0.6
LEOC	3.9	−1.1	1.9 ± 0.4
WAKA	5	−0.9	2.5 ± 0.4
VEXA	10.4	−0.6	3.6 ± 0.2
CNCL	11.4	−0.5	3.9 ± 0.2
PILK	13.8	−0.9	3.8 ± 0.4
MAKA	16.3	−1.3	4.8 ± 0.9
REDD	17.6	−0.6	4.0 ± 0.2
MCKE	22.7	−0.4	4.8 ± 0.3
NETT	28.8	−0.6	2.7 ± 0.4
HORN	32.8	−0.3	5.5 ± 0.3
BNET	44.4	−0.3	3.1 ± 0.3
MTCX	52	−0.3	0.7 ± 0.5
MTJO	68	−0.7	0.3 ± 0.2
MQZG	141.9	−0.8	−1.0 ± 0.3
OUSD	244.1	−0.5	0.0 ± 0.2

[a]Bold type indicates sites that have been continuous for most of their existence. HOKI, MQZG and OUSD are coastal sites off the main transect. Uncertainty estimates are ±1σ.

[b]Bernese processing, regional filtering using HOKI, QUAR, MTJO and OUSD as reference stations, and maximum likelihood estimation using white + power-law noise model. Annual cycles estimated at all sites, plus semi-annual at NETT and PILK.

(Table 1) and average 0.3 mm/yr for continuous and 0.4 mm/yr for semi-continuous sites.

[12] We establish a local reference frame for vertical velocity by adding a constant to the estimated rates to make the OUSD rate equal zero. OUSD is the site least likely to be affected by crustal deformation, and therefore the most likely to provide vertical rates relative to one of the adjacent plates, in this case the Pacific. Because this reference frame depends on only one site, whose rate may be biased, it is permissible when comparing observed and predicted rates (Figure 3) to shift the observed rates by as much as ±0.5 mm/yr. Independent analysis of some of the sites as part of a global solution using gamit/globk software [*Herring et al.*, 2006] gives vertical rates relative to OUSD that agree within uncertainty with those in Table 1.

5. Discussion

5.1. Observed Vertical Rates

[13] The vertical rates (Figure 3) show a generally consistent pattern, with low values on the west coast growing to a maximum of ~5 mm/yr near the highest topography, then decreasing to low values by MTJO. The most significant deviation from a smooth profile is at stations NETT and HORN.

[14] NETT is located in apparently solid bedrock on the lip of a U-shaped glacial valley with a fall of 1,400 m into the valley below at an average slope of 20°, but significantly steeper near the top. Because of concerns about NETT, including a large seasonal cycle (Table S2) and significant down-time during the winter, we established a lower elevation station (HORN) a few hundred m above the valley floor on a spur leading off the valley wall. Although HORN has much smaller seasonal variability, it shows a vertical rate significantly different from NETT's. Elastic surface loading calculations using estimates of the present-day rate of ice loss from Tasman Glacier, whose terminus is ~12 km NNE of HORN, predict a vertical rate of +0.3 to as much as +1 mm/yr at HORN, and somewhat slower at NETT (auxiliary material). Correcting for this effect would make HORN more consistent with the trend defined by MCKE, BNET and MTJO in Figure 3, leaving NETT as an unexplained outlier.

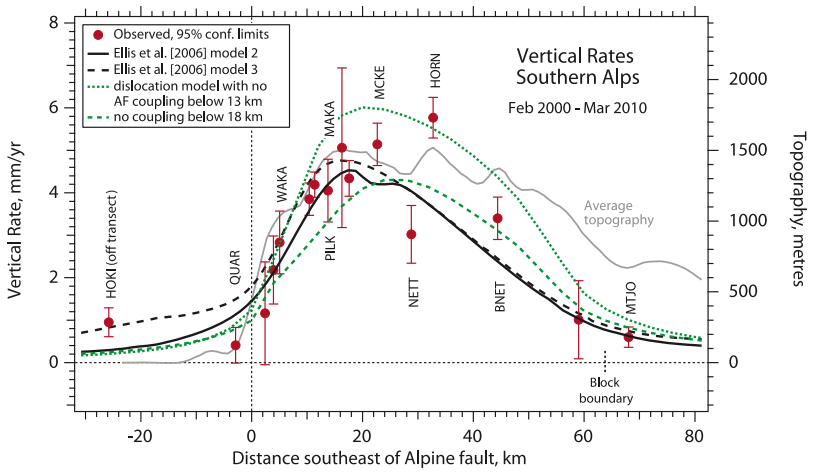

Figure 3. Relative vertical velocity profile across the Southern Alps from the west coast to the eastern foothills. Observed values (dots with 95% confidence limits) are shifted by +0.3 mm/yr relative to those in Table 1. Lines show predictions of interseismic vertical rate from elastic dislocation models (green) using two different coupling distributions (see text) on the 45°-dipping Alpine Fault [*Wallace et al.*, 2007; *Beavan et al.*, 2007] and from numerical models with more realistic rheological and temperature structures (black) [*Ellis et al.*, 2006]. In dislocation models the SE block boundary dips ~60° NW, with a coupling factor of 0.9–1 to 25 km depth and zero below. Solid grey line shows smoothed topography along the transect. Unlabelled sites may be identified using Table 1.

[15] Two major earthquakes (Figure 1) may have affected the time series. We observed no vertical coseismic offsets from the 2004 M_W 8 Macquarie strike-slip earthquake [*Watson et al.*, 2010]. Postseismic deformation due to mantle flow may be affecting vertical velocities in the Southern Alps, but insofar as it is common mode across our network, it will have been removed during regional filtering. Visual inspection (Figure 2) suggests an increase in vertical velocity at NETT and HORN from about 2005, but since this is not apparent at other sites, we infer it is not due to the Macquarie earthquake. The M_W 7.8 Dusky Sound (Fiordland) earthquake of 15 July 2009 generated coseismic vertical signals of a few mm that are largely common mode and therefore strongly attenuated by regional filtering.

5.2. Comparison With Model Calculations

[16] *Wallace et al.* [2007] use a model with elastic blocks rotating about vertical axes to interpret the 1994–2002 horizontal velocity field. Near our network, one block boundary follows the Alpine Fault and another follows faults distributed through the eastern foothills of the Southern Alps (Figure 1). The method solves simultaneously for rotation rates and elastic strains resulting from interseismic coupling that varies spatially along strike and down dip on the block-bounding faults. Rotation rates between the blocks are assumed to represent long-term motion. *Wallace et al.* [2007] find deeper coupling on the 45° dipping Alpine Fault than did *Beavan et al.* [1999], with the coupling factor decreasing from 1 at the surface to 0.7 by 8 km depth, remaining steady at 0.7 to 18 km, then trending linearly to zero by 25 km depth. *Beavan et al.* [2007, Plate 3c] find a reasonable fit to observed horizontal velocities when they re-model the same 1994–2002 velocity field forcing the coupling to trend to zero between 13 and 18 km depth, but a poor fit when the trend to zero is between 7 and 13 km.

[17] We use the distribution of slip deficit rate and direction on each of the block bounding faults, along with their defined strikes, dips and locations, in a back-slip dislocation model [*Savage*, 1983] to predict the vertical rate distribution along a profile through the GPS network (Figure 3). At the northwestern end of the profile, where the Alpine Fault has the greatest influence, most observed rates lie between the two dislocation model curves, which differ in that Alpine Fault coupling trends to zero over either the 7–13 km or the 13–18 km depth range. This suggests coupling on the Alpine Fault has fallen to zero by between 13 and 18 km depth. As the dip of the southeastern block boundary is not defined well by the horizontal velocity data [e.g., *Beavan et al.*, 2007, Plate 4], we choose its dip to make the long-term vertical rates across the two boundaries approximately equal, which leads to a near zero vertical rate between far-field locations on either side of the mountains (Figure 3). The resulting long-term vertical rate of the Southern Alps block is 5–6.5 mm/yr. This "tuning" of the model does not significantly affect the shapes of the model curves within 20–25 km of the Alpine Fault, and therefore does not affect our conclusions about Alpine Fault coupling.

[18] We also consider an alternative model in which faults southeast of the mountains are not pre-defined. *Ellis et al.* [2006] model the Alpine Fault earthquake cycle using a rheological structure, temperature distribution, and boundary conditions based on recent geophysical experiments. After a model conditioning period earthquakes are imposed every 500 years, with their coseismic slip magnitude and depth distribution dependent on the material properties and temperature distribution in the model. Stress transfer in the mid-crust causes shear strain during the interseismic period on a downward continuation of the coseismic fault, and also to a lesser extent along the boundary between the descending and overriding plates to the east. Figure 3 shows vertical rate profiles late in an interseismic period from Ellis et al.'s models 2 and 3, which differ in that model 3 has a steeper geothermal gradient than model 2; both models include a narrow (20 km) deforming zone in the mantle. The mantle deformation and the shear extending to the east between the plates causes the broadening of the observed surface deformation field to the east, whereas in the block models this is generated by variable slip on the eastern block boundary. Ellis et al.'s model 2, with the less-steep geothermal gradient, matches the observed vertical rates in the vicinity of the Alpine Fault better than their model 3.

6. Conclusions

[19] We have measured relative vertical components of velocity across the Southern Alps with precisions of 0.2–0.9 mm/yr (1σ) using up to 10 years of continuous and semi-continuous GPS data. The highest rates, ~5 mm/yr relative to the east coast, occur either side of the crest of the Southern Alps and ~20–30 km southeast of the Alpine Fault.

[20] These rates can be explained by long-term motions between coherent crustal blocks with superimposed elastic strains from interseismic coupling on the block-bounding faults, estimated using the much more extensive horizontal velocity field. How the motion is absorbed at depths below the crustal blocks is not resolved.

[21] The observed vertical velocity distribution suggests that interseismic coupling on the Alpine Fault falls to zero by 13 to 18 km depth, which is shallower than recent interpretations from horizontal GPS velocities but deeper than the 5–8 km locking depth derived from an earlier interpretation. With current vertical velocity uncertainties we are unable to distinguish between purely elastic models and those with more complex rheology.

[22] **Acknowledgments.** We thank Susan Ellis for her review of the manuscript, two anonymous reviewers for their suggestions and Chris Pearson for his help in setting up the project. The project has been supported by the NZ Foundation for Research, Science and Technology and by NSF (grants EAR-9903183 & EAR-9912071). Installation of the GPS equipment was supported by UNAVCO, who also archive the data.

References

Batt, G. E., and J. Braun (1999), The tectonic evolution of the Southern Alps, New Zealand: Insights from fully thermally coupled dynamical modeling, *Geophys. J. Int.*, *136*, 403–420, doi:10.1046/j.1365-246X.1999.00730.x.

Beaumont, C., P. J. Kamp, J. Hamilton, and P. Fullsack (1996), The continental collision zone South Island, New Zealand: Comparison of geodynamical models and observations, *J. Geophys. Res.*, *101*, 3333–3359, doi:10.1029/95JB02401.

Beavan, J. (2005), Noise properties of continuous GPS data from concrete-pillar geodetic monuments in New Zealand, and comparison with data from U.S. deep drilled braced monuments, *J. Geophys. Res.*, *110*, B08410, doi:10.1029/2005JB003642.

Beavan, J., et al. (1999), Crustal deformation during 1994–1998 due to oblique continental collision in the central Southern Alps, New Zealand,

and implications for seismic potential of the Alpine fault, *J. Geophys. Res.*, *104*(B11), 25,233–25,255, doi:10.1029/1999JB900198.

Beavan, J., P. Tregoning, M. Bevis, T. Kato, and C. Meertens (2002), The motion and rigidity of the Pacific Plate and implications for plate boundary deformation, *J. Geophys. Res.*, *107*(B10), 2261, doi:10.1029/2001JB000282.

Beavan, R. J., D. W. Matheson, P. Denys, M. Denham, T. Herring, B. Hager, and P. Molnar (2003), A vertical deformation profile across the Southern Alps, New Zealand, from 3.5 years of continuous GPS data, in *Proceedings of the Workshop: The State of GPS Vertical Positioning Precision: Separation of Earth Processes by Space Geodesy, April 2–4, 2003, Luxembourg. Luxembourg: European Centre for Geodynamics and Seismology, Cah. Cent. Eur. Geodyn. Seismol.*, *23*, 111–123.

Beavan, J., S. Ellis, L. Wallace, and P. Denys (2007), Kinematic constraints from GPS on oblique convergence of the Pacific and Australian plates, Central South Island, New Zealand, in *A Continental Plate Boundary: Tectonics at South Island, New Zealand*, *Geophys. Monogr. Ser.*, vol. 175, edited by D. Okaya et al., p. 75–94, AGU, Washington, D. C.

Cande, S., and J. Stock (2004), Pacific-Antarctic-Australia motion and the formation of the Macquarie Plate, *Geophys. J. Int.*, *157*, 399–414, doi:10.1111/j.1365-246X.2004.02224.x.

Dach, R., U. Hugentobler, P. Fridez, and M. Meindl (2007), *Bernese GPS Software Version 5.0*, 612 pp., Astron. Inst., Univ. of Bern, Bern.

DeMets, C., R. G. Gordon, and D. F. Argus (2010), Geologically current plate motions, *Geophys. J. Int.*, *181*, 1–80, doi:10.1111/j.1365-246X.2009.04491.x.

Ellis, S., J. Beavan, D. Eberhart-Phillips, and B. Stöckhert (2006), Simplified models of the Alpine Fault seismic cycle: Stress transfer in the mid-crust, *Geophys. J. Int.*, doi:10.1111/j.1365-246X.2006.02917.x.

Herring, T. A., R. W. King, and S. C. McClusky (2006), Introduction to GAMIT/GLOBK Release 10.3, Dep. Earth Atmos. Planet. Sci., Mass. Inst. of Technol., Cambridge.

Kohler, M. D., and D. Eberhart-Phillips (2003), Intermediate-depth earthquakes in a region of continental convergence: South Island, New Zealand, *Bull. Seismol. Soc. Am.*, *93*, 85–93, doi:10.1785/0120020043.

Koons, P. O. (1989), The topographic evolution of collisional mountain belts: A numerical look at the Southern Alps, New Zealand, *Am. J. Sci.*, *289*, 1041–1069.

Leitner, B., D. Eberhart-Phillips, H. Anderson, and J. L. Nabelek (2001), A focused look at the Alpine Fault, New Zealand: Focal mechanisms and stress observations, *J. Geophys. Res.*, *106*, 2193–2220, doi:10.1029/2000JB900303.

Okaya, D., T. Stern, and F. Davey (Eds.) (2007), *A Continental Plate Boundary: Tectonics at South Island, New Zealand*, *Geophys. Monogr. Ser.*, vol. 175, AGU, Washington, D. C.

Reyners, M. (1987), Subcrustal earthquakes in the Central South Island, New Zealand, and the root of the Southern Alps, *Geology*, *15*, 1168–1171, doi:10.1130/0091-7613(1987)15<1168:SEITCS>2.0.CO;2.

Savage, J. C. (1983), A dislocation model of strain accumulation and release at a subduction zone, *J. Geophys. Res.*, *88*, 4984–4996, doi:10.1029/JB088iB06p04984.

Stern, T., P. Molnar, D. Okaya, and D. Eberhart-Philips (2000), Teleseismic P wave delays and modes of shortening the mantle lithosphere beneath South Island, New Zealand, *J. Geophys. Res.*, *105*, 21,615–21,631, doi:10.1029/2000JB900166.

Sutherland, R., F. Davey, and J. Beavan (2000), Plate boundary deformation in South Island, New Zealand, is related to inherited lithospheric structure, *Earth Planet. Sci. Lett.*, *177*, 141–151, doi:10.1016/S0012-821X(00)00043-1.

Sutherland, R., et al. (2007), Do great earthquakes occur on the Alpine fault in central South Island, New Zealand?, in *A Continental Plate Boundary: Tectonics at South Island, New Zealand*, *Geophys. Monogr. Ser.*, vol. 175, edited by D. Okaya et al., pp. 235–251, AGU, Washington D. C.

Wallace, L. M., J. Beavan, R. McCaffrey, and K. Berryman (2007), Balancing the plate motion budget in the South Island, New Zealand, using GPS, geological and seismological data, *Geophys. J. Int.*, *168*, 332–352, doi:10.1111/j.1365-246X.2006.03183.x.

Wannamaker, P. E., G. R. Jiracek, J. A. Stodt, T. G. Caldwell, V. M. Gonzalez, J. D. McKnight, and A. D. Porter (2002), Fluid generation and pathways beneath an active compressional orogen, the New Zealand Southern Alps, inferred from magnetotelluric data, *J. Geophys. Res.*, *107*(B6), 2117, doi:10.1029/2001JB000186.

Watson, C., R. Burgette, P. Tregoning, N. White, J. Hunter, R. Coleman, R. Handsworth, and H. Brolsma (2010), Twentieth century constraints on sea level change and earthquake deformation at Macquarie Island, *Geophys. J. Int.*, *182*, 781–796, doi:10.1111/j.1365-246X.2010.04640.x.

Wdowinski, S., Y. Bock, J. Zhang, P. Fang, and J. F. Genrich (1997), Southern California Permanent GPS Geodetic Array: Spatial filtering of daily positions for estimating coseismic and postseismic displacements induced by the 1992 Landers earthquake, *J. Geophys. Res.*, *102*(B8), 18,057–18,070, doi:10.1029/97JB01378.

Wellman, H. W. (1979), An uplift map for the South Island of New Zealand, and a model for uplift of the Southern Alps, *Bull. R. Soc. N. Z.*, *18*, 13–20.

Williams, S. D. P. (2008), CATS: GPS coordinate time series analysis software, *GPS Solut.*, *12*, 147–153, doi:10.1007/s10291-007-0086-4.

Williams, S. D. P., Y. Bock, P. Fang, P. Jamason, R. Nikolaidis, L. Prawirodirdjo, M. Miller, and D. Johnson (2004), Error analysis of continuous GPS position time series, *J. Geophys. Res.*, *109*, B03412, doi:10.1029/2003JB002741.

J. Beavan, GNS Science, PO Box 30-368, Lower Hutt 5011, New Zealand. (j.beavan@gns.cri.nz)

M. Denham and P. Denys, School of Surveying, Otago University, PO Box 56, Dunedin 9010, New Zealand.

B. Hager and T. Herring, Earth, Atmospheric, and Planetary Sciences, Massachusetts Institute of Technology, 77 Massachusetts Ave., Cambridge, MA 02139, USA.

P. Molnar, Department of Geological Sciences, University of Colorado at Boulder, Boulder, CO 80309, USA.